Cell, Vol. 94, 715–725, September 18, 1998, Copyright ©1998 by Cell Press

Tumor Induction of VEGF Promoter Activity in Stromal Cells

Dai Fukumura,[1,7] Ramnik Xavier,[2,5,7] Takeyuki Sugiura,[5] Yi Chen,[1] Eun-Chung Park,[3] Naifang Lu,[5] Martin Selig,[4] Gunnlaugur Nielsen,[4] Tatyana Taksir,[4] Rakesh K. Jain,[1,6] and Brian Seed[5,6]

[1]Edwin L. Steele Laboratory
Department of Radiation Oncology
[2]Gastrointestinal Unit
[3]Melvin B. and Barbara K. Nessel Gene Therapy Center
[4]Department of Pathology
[5]Department of Molecular Biology
Massachusetts General Hospital
Boston, Massachusetts 02114

Summary

We have established a line of transgenic mice expressing the *A. victoria* green fluorescent protein (GFP) under the control of the promoter for vascular endothelial growth factor (VEGF). Mice bearing the transgene show green cellular fluorescence around the healing margins and throughout the granulation tissue of superficial ulcerative wounds. Implantation of solid tumors in the transgenic mice leads to an accumulation of green fluorescence resulting from tumor induction of host VEGF promoter activity. With time, the fluorescent cells invade the tumor and can be seen throughout the tumor mass. Spontaneous mammary tumors induced by oncogene expression in the VEGF-GFP mouse show strong stromal, but not tumor, expression of GFP. In both wound and tumor models the predominant GFP-positive cells are fibroblasts. The finding that the VEGF promoter of nontransformed cells is strongly activated by the tumor microenvironment points to a need to analyze and understand stromal cell collaboration in tumor angiogenesis.

Introduction

The neovascularization of solid tumors facilitates their growth and metastasis by providing nutrient flow and a frequently incomplete, fenestrated endothelial barrier between neoplastic cells and circulation (Fidler, 1995; Hanahan and Folkman, 1996; Jain, 1997). The new blood vessels that develop within solid tumors are thought to arise as a result of the proliferation and migration of endothelial cells from existing vasculature supplying the tumor bed in a complex process that involves the regulated interaction of several soluble mediators and their cognate receptors (Hanahan, 1997; Risau, 1997). Although the mechanisms by which endothelial cells are recruited to the tumor are not completely understood, it is well documented that virtually all malignant cells in culture express significant levels of at least one polypeptide mitogenic for endothelial cells, including vascular endothelial growth factor/vascular permeability factor (Ferrara and Davis-Smyth, 1997), basic fibroblast growth factor (bFGF), and other cytokines that promote endothelial cell proliferation (Fidler, 1995; Friesel and Maciag, 1995).

As the neoplastic cells of solid tumors proliferate, they develop a complex association with the surrounding nonneoplastic tissue that is suggestive of an abnormal genesis of solid tissue with its associated matrix, tissue stromal cells, and vascular supply (Dvorak et al., 1995). Similarities between the stroma of tumors and wounds has led to the suggestion that tumors can be thought of as wounds that do not heal (Dvorak, 1986). At present the factors that regulate the development of the nonmalignant constituents of tumors, as well as the influences these constituents exert on the neoplastic compartment, are poorly understood (Helmlinger et al., 1997; Jain, 1997). In large measure the scarcity of information about the regulatory circuits that control the interplay between tumor and stroma can be attributed to the difficulty of simulating the tumor microenvironment in vitro.

To begin to study the interactions that lead to tumor angiogenesis, we have created and analyzed transgenic mice that express an engineered version of GFP under the control of the human VEGF promoter. In these mice VEGF promoter activation associated with normal wound repair is manifested by fluorescence developing at the wound margins and extending throughout the granulation tissue. Following implantation of solid tumors, intensely fluorescent fibroblasts can be observed surrounding and infiltrating the tumor mass. When spontaneous mammary tumors in the VEGF-GFP background are examined, GFP can be found in fibroblasts surrounding the neoplastic nodules but not in the tumor cells themselves.

Results

A reporter for VEGF promoter activity was prepared in which an engineered GFP was placed immediately downstream of 2.85 kb of VEGF promoter and 5′ untranslated region. To reduce integration site dependence the transcription unit was inserted between tandem copies of the core AT-rich element of the matrix attachment region located 3′ to the human beta globin locus. Three pups surviving to maturity were found to be transgenic by analysis of DNA prepared from tail sections and were tested for acquisition of green fluorescence around the margins of a lesion generated by a small full-thickness wound of one ear. All three animals showed similar responses, but the signal was weak in two. The mouse with the best response was then mated to generate the transgenic line.

Figures 1a and 1b show transmission and fluorescence images obtained by intravital microscopy of a healing full-thickness circular incision in the ear of the

[6]To whom correspondence should be addressed.
[7]These authors contributed equally to this work.

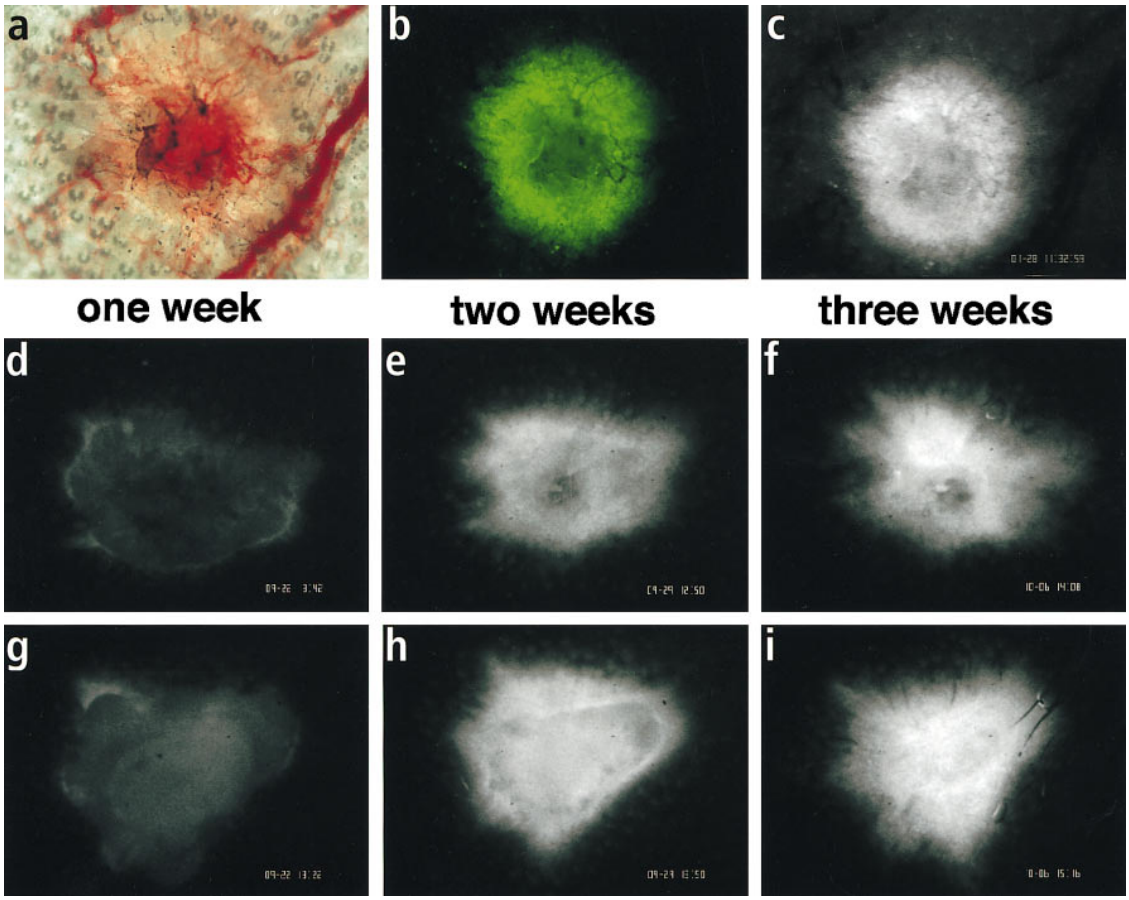

Figure 1. VEGF Promoter Activity during Wound Healing in Transgenic Mice

(a–c) Low power microscopic images of a full-thickness wound in the ear of VEGF-GFP transgenic founder 2 weeks after the wound creation. Transillumination (a) and GFP fluorescence (b and c) images were either photographed (a and b) with ASA 400 film or acquired with the aid of an intensified CCD camera (c). (c) is shown to illustrate the relative intensities of signal observed with the CCD camera and conventional film.

All subsequent images (d–i) were recorded digitally and represent GFP expression during wound healing of VEGF-GFP transgenic mice (FVB-C3H F1 hybrid) 1 week (d and g), 2 weeks (e and h), and 3 weeks (f and i) after wound creation. The fluorescence images were digitized and processed at the same instrument settings. One week after the wound creation, weak GFP fluorescence was observed predominantly at the margins of the wound (d and g). Only a few newly formed vessels can be seen localized at the periphery of the wound. Two weeks after wound creation, the GFP fluorescence is brighter and more localized toward the center of the wound (b, c, e, and h). Angiogenesis can be observed in the wound, especially in the peripheral region (a). Three weeks after the wound creation, GFP fluorescence is further increased and advanced toward the center of the wound (f and i). The bar (a) represents 500 μm, and the same scale applies to all panels.

founder mouse. Around the incision margins can be seen distinct green fluorescence arising from local activation of the reporter gene in response to wound-elicited factors. The color images shown in Figure 1 were acquired at day 14 postwounding. In the first few days after wound creation a thick scab was observed on the wound. Because the scab showed significant autofluorescence, it was difficult to observe GFP-specific fluorescence while it was present. The scab disappeared about 1 week after wound creation, and the wound was then seen to be partially filled in with granulation tissue. Two examples of the characteristic time course of GFP expression following full-thickness wounds in founder progeny are shown in the lower panels of Figure 1. Weak GFP fluorescence was observed predominantly at the margins of the wound 1 week after wound creation (Figures 1d and 1g). Only a few newly formed vessels could be seen, localized at the wound periphery (not shown). Two weeks after wound creation, the GFP fluorescence was brighter and had advanced toward the center of the wound (Figures 1b, 1c, 1e, and 1h). More prominant angiogenesis was observed at this time, especially at the wound periphery (Figure 1a). Three weeks after wound creation, GFP fluorescence was further increased and had continued to advance toward the center of the wound. Observation was discontinued before the ulcers that formed at the wound site had completely healed.

GFP is a sensitive reporter because it is easily detected, cell-restricted, and stable. The fluorescence intensity of cells expressing the GFP reporter is a convolution of transcript creation with the decay functions for both mRNA and protein over the natural lifetime of GFP in vivo. To estimate the relevant parameters, we transfected cells of the U87 (human glioma) and LS174T (human colon adenocarcinoma) cell lines with a construct bearing the GFP expression cassette described above

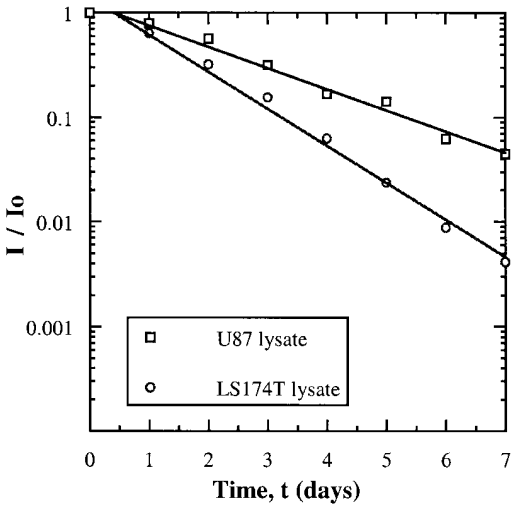

Figure 2. GFP Turnover in Mammalian Cells in Culture

Total fluorescence at 510 nm of lysates prepared from U87 (human glioma) and LS174T (human colon adenocarcinoma) cells transfected with GFP under the control of a tetracycline-sensitive promoter. At time 0, tetracycline was added to inactivate the promoter. The ratio of the fluorescence intensity I to the initial fluorescence intensity I_0 is shown. The lines fit to the data were generated by a linear least squares regression and are satisfied by the equations $I/I_0 = 1.209e^{-0.468t}$ and $I/I_0 = 1.402e^{-0.818t}$ (t in days), corresponding to GFP terminal half-lives of 1.48 and 1.18 days in U87 and LS174T cells, respectively.

under the control of a synthetic tetracycline-responsive promoter (Gossen and Bujard, 1992). Following growth in culture under conditions in which the GFP was fully induced, tetracycline was added to the medium to inactivate the promoter, and the total fluorescence activity of the culture was determined at various times thereafter. The recorded values thus provide a measure of fluorescence independent of cell proliferation and, hence, independent of dilution effects attributable to increases in cell size or number. Figure 2 shows that the fluorescence of lysates prepared from the two transfected cell types declined with terminal half-lives of 35.5 hr and 28.3 hr for U87 and LS174T, respectively. The ordinate intercepts were greater than unity in both cases, consistent with a delay between removal of tetracycline and initiation of decay that was in strikingly good agreement between the two cell lines, 9.6 hr for U87 and 9.8 hr for LS174T. Assuming that this lag represents the effective interval for termination of production (i.e., assimilates the time required for both cessation of promoter activity and decay of mRNA), GFP in mammalian cells in culture has an estimated half-life of between 1.2 and 1.5 days. If similar characteristics are applicable to cells in vivo, the observed GFP intensity in the photomicrographs represents the integral of promoter activity over a natural (exponential) decay interval of approximately 2 days.

To evaluate VEGF promoter activity in the context of tumor development, we produced hybrid mice by mating FVB-derived, VEGF-GFP transgenic animals with wild-type C3H mice. The resulting animals can serve as hosts for well-studied C3H-derived tumor lines. Tumors from two such lines, the mammary carcinoma MCaIV and the hepatocellular carcinoma HCaI, were implanted subcutaneously in dorsal skin chambers attached to transgenic F1 hybrids. Although the distribution and time course of fluorescence are different for the two tumors, fluorescence generally first appears at the margins (Figures 3b, 3c, 3e, and 3h) and penetrates into the tumor mass (Figures 3f, 3i, and 3l). In the mammary carcinoma, strong fluorescence can often be seen retained about the periphery (e.g., Figure 3c). Dense vascularization occasionally limits fluorescence detection (Figure 3l).

Over a longer period of time, the mammary carcinoma organizes and evolves along a somewhat different path than the hepatoma (Figure 4). Although initially the fluorescent cells are seen exclusively at the tumor periphery, the fluorescent cells appear to penetrate quickly into the HCaI tumors. An example of fluorescence flare during the establishment of such a tumor is shown in the bottom row of Figure 4. In this sequence a period of intense fluorescence is followed by a diminution of signal intensity as neovasculature appears. It seems likely that this progression reflects a local oxygen and/or nutrient demand that subsides as the need for vasculature is satisfied. Whatever the cause, dense vascularization ensues and the signal drops quickly (compare 4i and 4l with 4h and 4k). In contrast, the MCaIV tumors in this series continued to show intense fibrous fluorescence that came to colocalize with vascular bundles (Figure 4c and 4f).

Because contributions from fluorescence sources out of the focal plane make it difficult to distinguish cell shapes with precision, intravital confocal microscopy was undertaken. Using this approach, out-of-plane signal was greatly reduced, and similar patterns of cellular fluorescence could be seen around the margins of 3-week-old wounds or within implanted tumors 3 weeks postimplantation (Figure 5). Imaging of the tumor and wound at higher magnification showed that individual cells could be detected throughout the tumor mass. In both cases the fluorescent cells had the extended morphology that is characteristic of tissue fibroblasts (Figure 5).

Histologic examination of the implanted breast carcinoma and hepatocellular carcinoma at 1 week showed tumor nodules surrounded by fibroblastic proliferation with no extension into the tumor nodules (Figures 6a and 6f). The rim of fibroblast proliferation was in the region seen to be extensively populated with green fluorescent cells by confocal microscopy. Consistent with this, the fibroblasts from this portion of the section were positive on immunohistochemical staining with a polyclonal anti-GFP antibody (Figure 6e). At 3 weeks, the fibroblasts can be seen to extend from the periphery into the tumor bed, forming fibrous septae (Figures 6b-6d). Examination of the skin wound showed fibroblastic proliferation underneath the ulcer that fills the wound bed at 3 weeks (Figure 6g). No reepithelialization is present 1 week after wounding, and the fibroblasts adjacent to and beneath the wound show strong GFP immunoreactivity (Figure 6h). GFP-positive cells in tumor sections did not stain positive for CD31, a marker of small vessel endothelium, nor for CD45 (pan-hematopoietic cell), nor CD3 (T-lymphoid cell) markers (not shown). On Giemsa staining the few cells found to stain metachromatically were round to oval in shape, consistent with an identification as tissue mast cells. These cells were far less

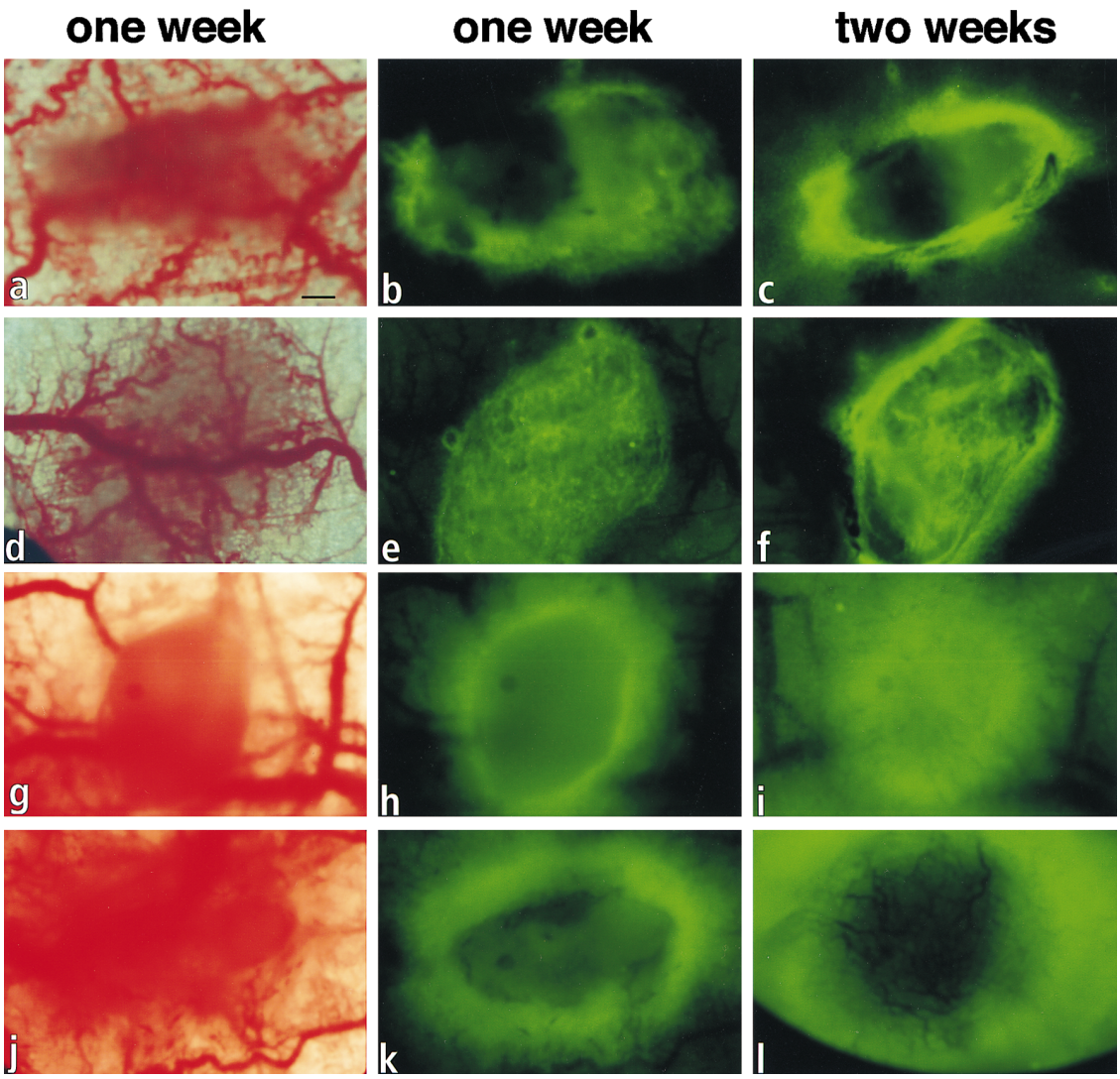

Figure 3. GFP Reporter Activity in Tumors Implanted in VEGF-GFP Transgenic Mice

Photomicrographs of MCaIV, a murine mammary carcinoma (a–f) and HCaI, a murine hepatoma (g–l), grown in dorsal skin chambers of VEGF-GFP transgenic mice. The left panels (a, d, g, and j) are transilluminated images at 1 week after tumor implantation, and the middle and right panels are the corresponding fluorescence images at 1 week (b, e, h, and k) and 2 weeks (c, f, i, and l) after the tumor implantation. One week after tumor implantation, marked vessel dilatation was observed in the host vessels surrounding or underneath the tumor xenografts (a and d). GFP fluorescence was initially localized at the tumor-host interface of HCaI tumors (h and k). Two weeks after the tumor implantation, the GFP fluorescence was intensified (c and d) and expanded (i and l). The vasculature in the tumor became apparent at this point. In general, the peripheral region of the tumor (tumor-host interface) shows stronger GFP fluorescence than the center. The bar in (a) represents 500 μm, and the same scale is used in all panels.

numerous than the fibroblasts. To make a definitive identification of the stromal cells, we prepared sections for electron microscopy (Figure 6i).

Ultrastructural examination of the 1 week tumor specimen (Figure 7a-7c) revealed proliferation of spindle-shaped cells adjacent to cohesive nests of tumor cells. The spindle-shaped cells have the features of primitive fibroblasts, containing abundant intracytoplasmic ribosomes, rough endoplasmic reticulum, few mitochondria, and pinocytotic vesicles (Figure 7b and 7c). They are arranged individually and enmeshed within a matrix containing occasional banded collagen-dilated fibers.

Examination of wound and tumor specimens at 2 weeks (Figures 7d-7h) also showed proliferation of fibroblasts. In these specimens the fibroblasts are more mature, containing abundant dilated and undilated rough endoplasmic reticulum and fewer ribosomes. The extracellular matrix contains more collagen fibers that are being secreted by the fibroblasts (Figures 7f and 7h). The spindle-shaped cells did not show intracytoplasmic granules and bore no prominent intracytoplasmic ribosomes, characteristic of mast cells/histiocytes and lymphoid cells, respectively.

To compare in vivo and in vitro properties, primary

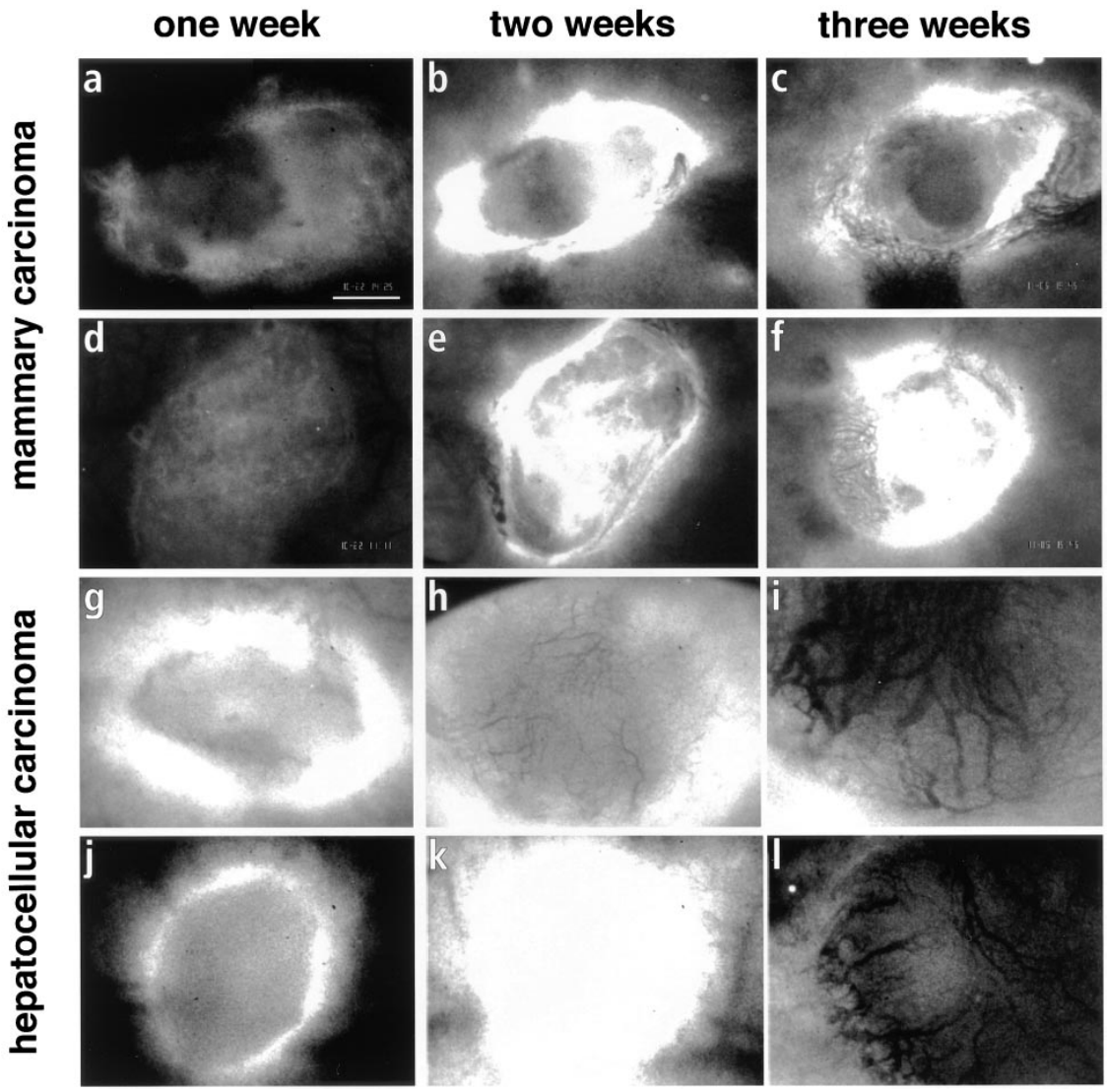

Figure 4. Time Course of GFP Expression during Tumor Growth in the VEGF-GFP Transgenic Mice

GFP fluorescence images of MCaIV tumors (a–f) and HCaI tumors (g–l) were acquired with a digital camera. Data were acquired under identical conditions in all panels. The left panels (a, d, g, and j), the middle panels (b, e, h, and k), and the right panels (c, f, i, and l) represent the same tumor at 1 week, 2 weeks, and 3 weeks after implantation, respectively. GFP fluorescence was generally more intense at the tumor periphery. Note the high degree of correlation between fluorescence and vasculature in (c) and (f). (i) and (l) show only a part of the tumor. The growth rate and angiogenesis varied between individual tumors and tumor types. The bar in (a) represents 1 mm in all panels.

embryo fibroblasts were prepared from VEGF-GFP mice and propagated in culture. Flow cytometry of cells grown in culture unexpectedly showed a bimodal pattern of constitutive GFP expression (Figure 8). The relative induction of the VEGF promoter under these conditions was determined by comparison of the signal intensities observed in vitro and in vivo. Tumors implanted in the VEGF-GFP mouse were excised, dissociated, and subjected to flow cytometry. Although the cell numbers were small, the fluorescence distribution of the cells recovered from the tumors coincided with the fluorescence distribution observed following cytometry of primary cells in culture (Figure 8). Thus, to the limit of experimental resolution, the VEGF promoter of fibroblasts in culture is induced as strongly as that of fibroblasts infiltrating implanted tumors. Measurement of the concentration of VEGF in the culture supernatant of fibroblasts prepared from transgene-positive and -negative mice showed that the ratio of production by positive cultures compared to negative cultures was 1.24 ± 0.25 ($n = 4$). Thus, there are no significant differences between the endogenous VEGF promoter activity of transgenic and nontransgenic fibroblasts. However, transgenic cultures tended to show a decrease in GFP frequency with time, which may reflect a selection against cells expressing high levels of GFP.

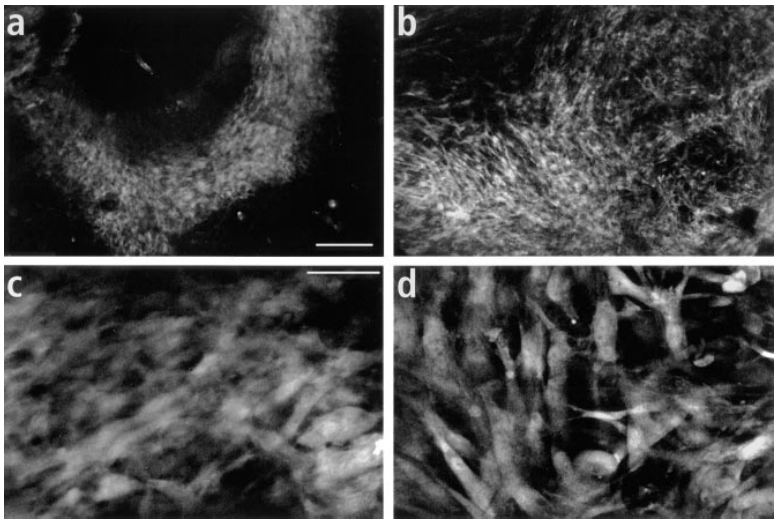

Figure 5. Confocal Microscopy of GFP Fluorescence in Both Wound and Tumor in the VEGF-GFP Transgenic Mice

GFP-positive cells were visualized by confocal laser microscopy. Both the wound in the ear (a and c) 3 weeks after the wound creation and MCaIV tumor grown in the dorsal skin chamber (b and d) 3 weeks after the tumor implantation showed spindle-shaped fluorescent cells.

The bar in (a) represents 200 μm, and the same magnification is shown in (b); the bar in (c) represents 50 μm, and the same magnification is shown in (d).

Mice bearing the VEGF-GFP transgene were mated with mice bearing the polyoma middle T antigen under the control of the mouse mammary tumor virus long terminal repeat promoter. Spontaneous multifocal mammary tumors have been shown to appear with high frequency in the latter mice (Guy et al., 1994). Mice transgenic for both the GFP and the middle T transgenes were found to develop multiple spontaneous mammary tumors at ages 4 to 5 months. The mice were sacrificed, and the lesions were examined for distribution of GFP by immunohistochemistry. In general the spontaneous tumors were similar in appearance and organization to the implanted MCaIV mammary carcinoma, with vascular plexi apparent in the perineoplastic stroma. No anti-GFP antibody reactivity was detected in the tumor nodules themselves, which were relatively avascular (Figure 9). In contrast the fibrotic tissue surrounding the nodules, which was hyperplastic and vascularized, showed numerous scattered cells reactive with anti-GFP antibody (Figure 9). Fibroblasts surrounding blood vessels traversing the stroma stained positive for GFP, whereas endothelial cells were negative (Figure 9).

Discussion

Understanding the factors that govern the growth and metastasis of solid tumors is an important but challenging objective. Much of the difficulty in understanding tumor dynamics comes from the complexity of the experimental systems in vivo and from the failure of in vitro culture models to faithfully reflect events taking place in an organismic context. In the studies reported here, intravital microscopy and a sensitive intracellular reporter have been exploited to increase our understanding of the interplay between neoplastic cells and the underlying stromal bed. Using a transgenic animal line in which the VEGF promoter drives the expression of GFP, we have been able to detect and track activation of the VEGF promoter in response to wounding and neoplasia.

VEGF transcriptional activation was a surprisingly long-lived phenomenon in both the wounds and tumors studied here. Strong GFP production associated with proliferation of mesenchymal elements could be seen for weeks following wounding or tumor implantation. The distribution and evolution of fluorescence appeared to follow a characteristic course for the two tumor types studied. The mammary carcinoma developed a more septated fluorescence that remained intense as the tumor grew, whereas the hepatocellular carcinoma developed a diffuse fluorescence that waned as dense vascularity ensued. Both tumor types showed extensive penetration of fluorescent cells into the tumor mass.

A similar picture was seen in the setting of spontaneous tumorigenesis in a transgenic oncogene model. GFP immunoreactivity was apparent around the margins of multifocal tumor nodules. No GFP reactivity was detectable in the nodules themselves, suggesting that VEGF promoter activity in the neoplastic cells was at best poorly induced. However, fibroblasts in the fibrotic tumor matrix were clearly positive for GFP.

Of the different mechanisms that regulate VEGF promoter strength, hypoxia (Shweiki et al., 1992) is best understood. However, in vivo measurements have shown that the partial oxygen pressure (pO_2) of tumor tissue and vasculature is heterogeneous and vessel perfusion rates do not necessarily correlate with local oxygenation (Helmlinger et al., 1997). Although malignant neoplasms can develop impressive vascularity, the vasculature is imperfect, disordered and leaky, and poorly conducts nutrients and erythrocytes through the tumor mass (Jain, 1997). As a result the tumor shows irregular, constantly changing patterns of metabolic demand that may be expected to induce cognate fluctuations in VEGF transcriptional activity.

VEGF mRNA accumulation in vivo is also regulated by prolongation of mRNA half-life through posttranscriptional regulatory events mediated by specific *cis*-sequences encoded in the mRNA 3′ untranslated region (Shima et al., 1995; Stein et al., 1995; Levy et al., 1996; Damert et al., 1997). Because the reporter construct

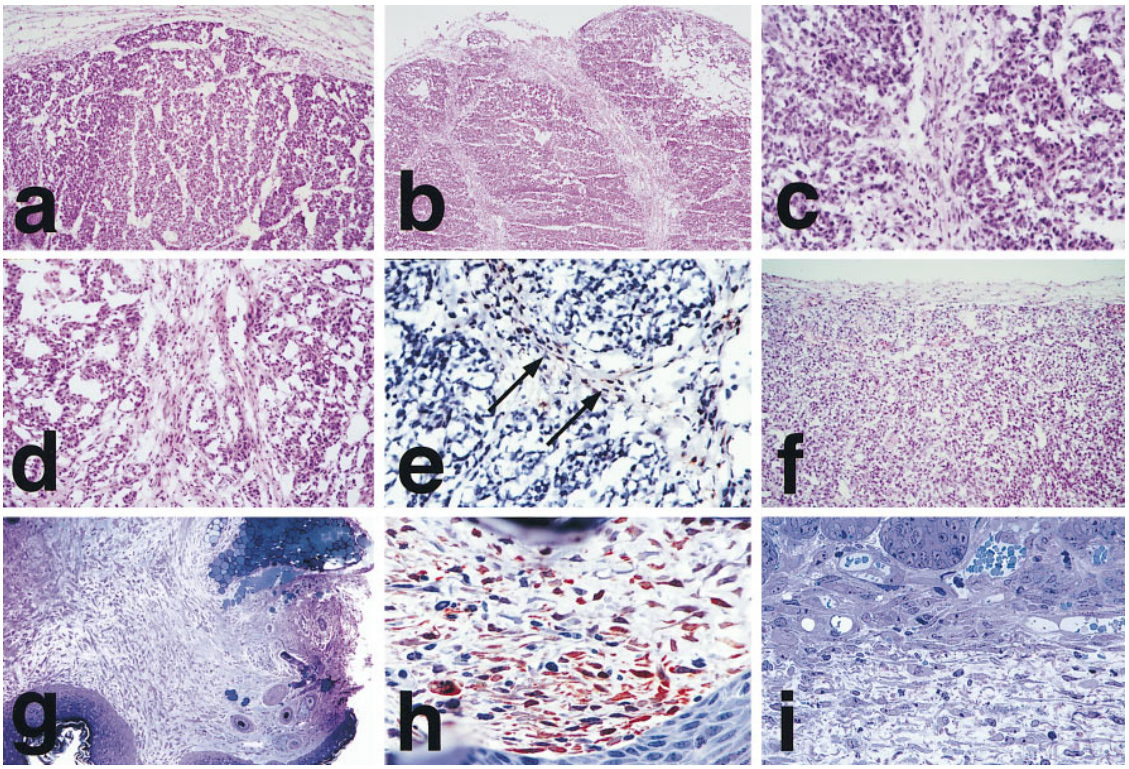

Figure 6. Light Microscopy of Mammary Carcinoma and Hepatocellular Carcinoma in VEGF-GFP Transgenic Mice

(a) Breast tumor implant at 1 week showing fibroblast proliferation (top) surrounding a tumor nodule (H&E).

(b) Same tumor at 3 weeks showing extension of the peripheral fibroblastic proliferation into the tumor nodule, forming fibrous septae (H&E).

(c and d) Higher power of the septae that are formed by bland spindle-shaped fibroblasts surrounded by pink collagenous matrix (H&E).

(e) Immunohistochemical stain for green fluorescent protein shows positive (red) cytoplasmic staining of the fibroblasts. The surrounding neoplastic cells are negative.

(f) Hepatocellular carcinoma implant after 1 week showing peripheral fibroblastic proliferation surrounding a tumor nodule. No extension of the fibroblastic proliferation into the tumor is present at this stage (H&E).

(g) One micrometer section of skin with surface wound (right) and underlying fibroblastic proliferation.

(h) Immunohistochemical stain for GFP shows intense cytoplasmic staining of the fibroblasts within the ear wound.

(i) A 1 μm section better illustrates the neoplastic cells (3 week tumor, top) and surrounding fibroblastic proliferation (Toluidine blue). Note marginal vessels with erythrocytes (blue).

described in this work does not contain the 3′ untranslated region, it does not assimilate mRNA stability effects.

In both normal wound recovery and neoplasia, the most prominent cells showing VEGF promoter activation are spindle-shaped cells that ultrastructurally display classic features of fibroblasts and do not show external lamina, junctions, tonofilaments, lumen formation, Weibel-Palade bodies, or other structural features suggestive of keratinocyte or endothelial cells. The cells are not sessile, but migrate into the wound or tumor, presumably under the influence of as-yet-unidentified chemotactic factors. Fibroblasts recovered from the tumor mass and analyzed by flow cytometry have the same fluorescence profiles as fibroblasts propagated in culture. We conclude from this that fibroblasts grown under standard conditions in vitro are as activated with respect to VEGF promoter activity as fibroblasts in tumors. This rather surprising observation suggests that culture in vitro is highly activating for VEGF promoter function and that additional effort will need to be expended to find culture conditions that mimic the status of normal (unactivated) tissue in vivo.

In normal rat primary fibroblasts grown in culture, hypoxia induces a G_0/G_1 checkpoint that results in growth arrest, whereas the same conditions cause transformed fibroblasts to undergo apoptosis (Graeber et al., 1994; Schmaltz et al., 1998). Because our findings point to a potentially important role for fibroblasts in VEGF production, the report that hypoxia induces growth arrest in vitro is unexpected and further suggests the importance of studying events in vivo. Similarly, the finding that fibroblasts in culture show highly induced VEGF transcriptional activity clearly indicates that other factors than hypoxia can significantly affect promoter strength.

VEGF is widely expressed in normal tissues (Berse et al., 1992), and its promoter region bears many of the characteristics of housekeeping genes (Tischer et al., 1991). Hence, it seems likely that in principle almost any cell type could serve as a source for VEGF upon hypoxic or ischemic demand. In the context of wound angiogenesis, previous studies have focused on the role of kera-

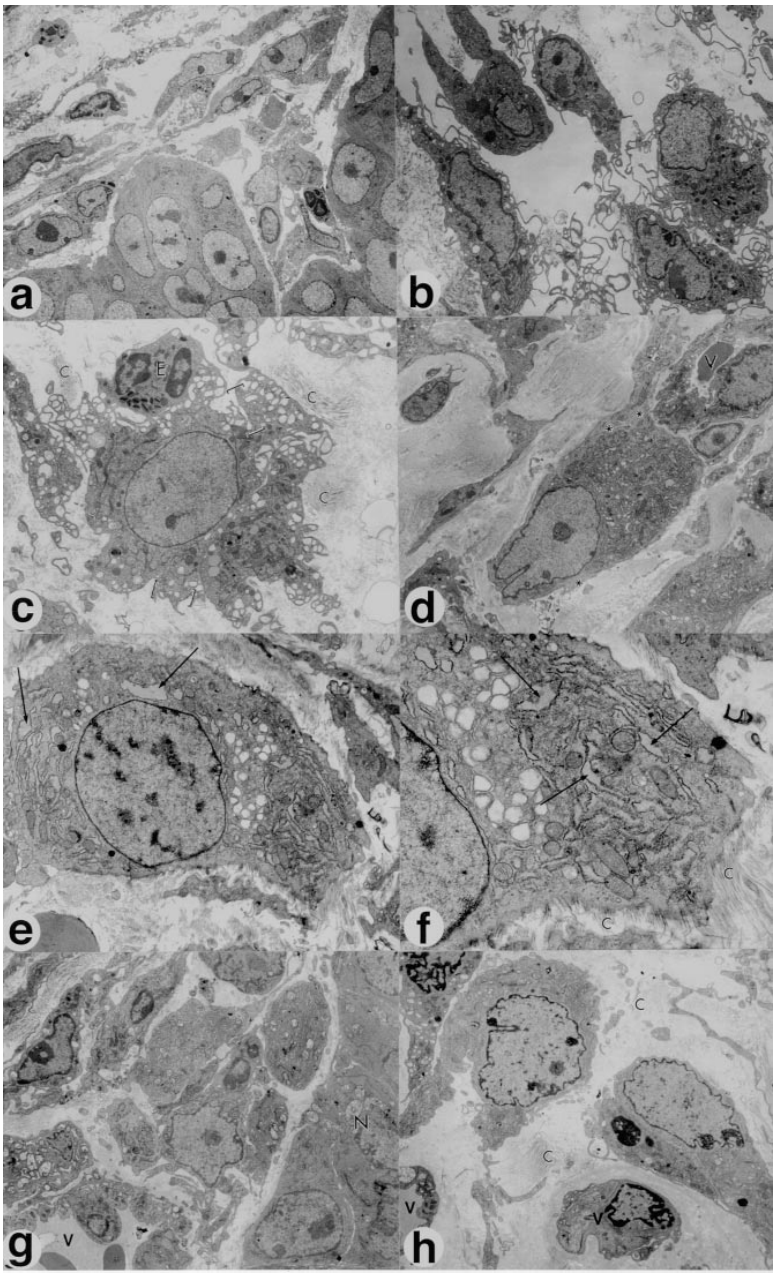

Figure 7. Electron Microscopy of Tumor and Wound Sections Showing High Fluorescence

(a) Tumor at 1 week. Low power showing spindle-shaped fibroblasts adjacent to cohesive nests of tumor cells (right and bottom).

(b and c) The fibroblasts have delicate cytoplasmic processes and contain abundant intracytoplasmic ribosomes, rough endoplasmic reticulum, occasional mitochondria, and pinocytic vesicles (brackets). Note the extracellular collagen deposition (C) and and an eosinophil (E) adjacent to the fibroblast.

(d) Ulcerative ear wound at 2 weeks. Fibroblasts with abundant rough endoplasmic reticulum and peripheral filaments (*). A vessel (V) is also present.

(e and f) Higher power showing abundant undilated and dilated rough endoplasmic reticulum (arrow). Surrounding the fibroblast are collagen fibers (C) that cross the cell surface and are being secreted by them.

(g) Mammary carcinoma at 2 weeks. Low power view showing cohesive clusters of neoplastic cells to the right (N) and discohesive proliferation of fibroblasts to the left. A vessel containing erythrocytes is present in the lower left (V).

(h) The spindle-shaped fibroblasts are arranged individually and are enmeshed within a matrix containing banded collagen fibers (C). Their cytoplasm contains abundant rough endoplasmic reticulum. Two capillary-sized vessels are also present.

Final Magnifications: (a), 1000×; (b), 1600×; (c), 2500×; (d), 1600×; (e), 3000×; (f), 5900×; (g), 1900×.

tinocytes. In culture these cells respond to growth factors and cytokines with increased VEGF production (Frank et al., 1995), and shorter term studies of epidermal wounds using in situ hybridization have identified them as a major source of VEGF transcripts (Brown et al., 1992). The wounds created in this study were ulcerative full-thickness excisions that generally showed little re-epithelialization and healed poorly. Imaging of GFP fluorescence during the period in which the keratinocyte contribution was previously reported to be dominant (Brown et al., 1992) proved difficult because of the high level of autofluorescence associated with scab formation. During the later granulation phase, few of the fluorescent cells appeared to be epithelial in origin, and the principal contribution to fluorescence in the granulation tissue can be attributed to fibroblasts. Although it is likely that more superficial wounds would show a greater keratinocyte involvement, it is significant that the wounds in this study did not heal well and that striking similarities were observed between the pattern of induction of VEGF promoter activity in the wounds and implanted tumors, consistent with the earlier suggestion that tumors behave as wounds that do not heal (Dvorak, 1986).

At present the relative contributions of tumor and stroma to endothelial cell proliferation and migration are not understood. Although data from in vitro measurements of VEGF production by tumor cells in culture have led to the assumption that the tumor is the principal if not sole source of VEGF, the results of this work point

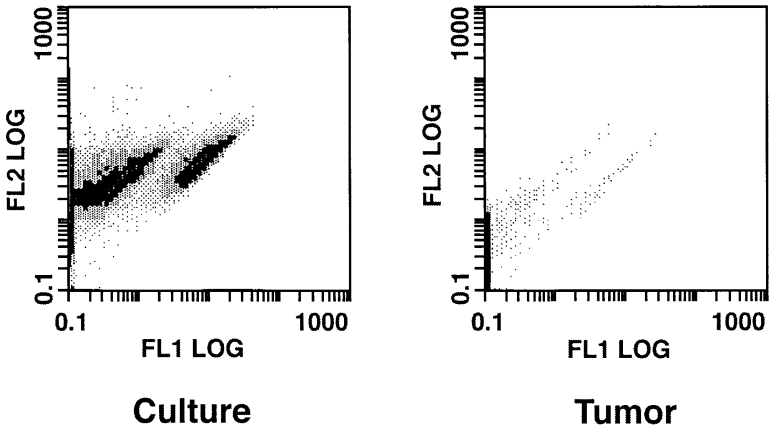

Figure 8. Cytometry of VEGF-GFP Fibroblasts Propagated in Culture or Excised from Tumors

Primary mouse embryo fibroblast cultures were initiated from transgenic animals and passaged in vitro. Cells analyzed by flow cytometry were found to exhibit a bimodal fluorescence distribution (left panel). Cells prepared by digesting tumor samples with collagenase and analyzing events in the scatter gate corresponding to fibroblasts showed a bimodal fluorescence pattern coincident with that of cells grown in culture (right panel).

to the possibility that stromal elements play an important role. Mammary fibroblasts from both tumor and normal breast tissue have been shown to produce VEGF in culture (Hlatky et al., 1994), and our findings indicate that fibroblasts from other sources likely behave similarly. The finding that stromal fibroblasts penetrate deep into implanted tumors raises the need to consider whether fibroblasts serve other functions besides production of VEGF, possibly including the production of chemotactic factors that elicit endothelial cell migration. In addition, it is presently unclear what fraction of neovascular growth can be attributed to VEGF as opposed to other polypeptides that have endothelial cell mitogenic potential, such as basic fibroblast growth factor.

Targeting antitumor therapy to stromal elements required for tumor growth may be a superior strategy for retarding the growth of solid neoplasms, since normal tissue is unlikely to show the genetic plasticity that often accompanies malignant transformation, a plasticity that allows transformed cells to rapidly acquire resistance to chemotherapeutic agents (Kerbel, 1991; Kim et al., 1993; Fidler, 1995; Parangi et al., 1996; Boehm et al., 1997). A better understanding of stromal contributions will likely increase our awareness of the importance of other molecules than VEGF in the growth of solid malignancies and may result in the identification of new therapeutic targets for future treatments focusing on the tumor stroma.

Experimental Procedures

Constructs and Reagents

Eight hundred base pairs of the core matrix attachment region from the human beta globin 3′ DNaseI hypersensitive site (Fleenor and Kaufman, 1993), comprising nucleotides 1601 to 2400 of GenBank X54282, were placed between MluI and SpeI sites upstream and between BamHI and NheI sites downstream of a GFP expression vector consisting of a codon-optimized GFP bearing two mutations (FS64LT) upstream of a human IgG1 intron and an SV40 polyadenylation sequence (Cormack et al., 1996; Haas et al., 1996; Heim and

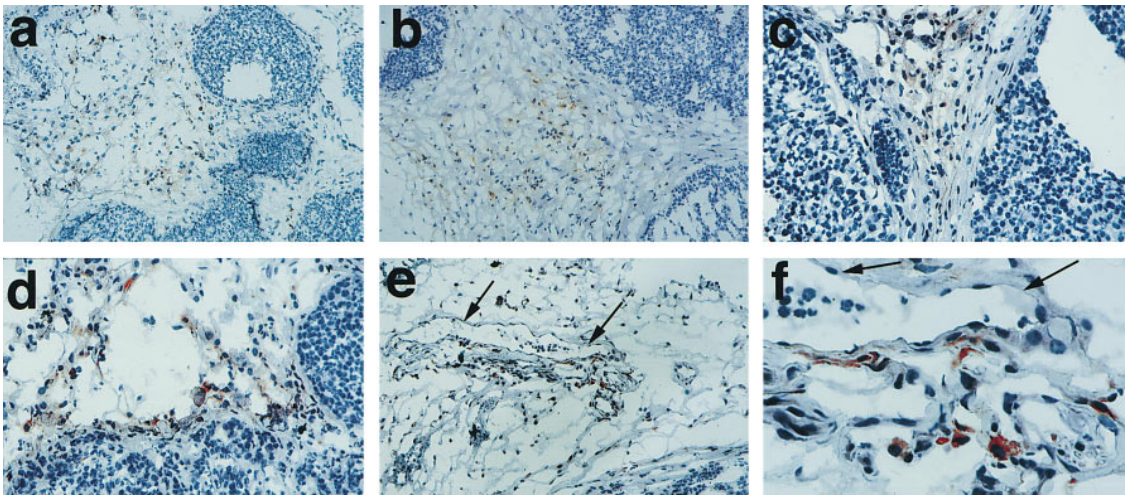

Figure 9. Immunohistochemistry of GFP in Spontaneous Tumors Arising in VEGF-GFP Mice Bearing an MMTV-Py mT Transgene

VEGF-GFP mice expressing the polyoma middle T antigen under the control of the MMTV LTR develop multifocal spontaneous mammary tumors (a–d). (a and b) Low power images showing positive reaction (red) with anti-GFP antibody by fibroblasts in the loose tumor stroma but not in the tumor nodules.

(c and d) Higher power images of tumor/stroma interface. Note absence of detectable reactivity within the tumor cells.

(e) Blood vessel (arrows) in tumor stroma surrounded by GFP-positive fibroblasts. Within the vessel are a few polymorphonuclear leukocytes.

(f) Magnified view of (e). The endothelial cells lining the vessel (arrows) do not react with anti-GFP antibody.

Tsien, 1996). VEGF promoter sequences from 552 to 3401 of GenBank M63971 (Tischer et al., 1991) were inserted between SpeI and HindIII to give the expression cassette.

Wound Preparation

Wounds were created using a modified technique previously described (Bondár et al., 1991). Mice were anesthetized with Ketamine 90 mg/kg (Parke-Davis, Morris Plains, NJ) and Xylazine 9 mg/kg (Fermenta, Kansas City, MO). Prior to excision, the overlying hair of the mouse ear was removed with a depilatory cream (Neet, Reckitt and Colman Inc., Wayne, NJ). The dorsal skin layer of the ear, down to but not including the cartilage, was excised with microscissors under a disecting microscope to provide a full-thickness wound of approximately 2 mm in diameter. One, two, and three weeks after wound creation, mice were anesthetized, the ears with the healing wound were gently placed on the transparent observation platform, and a thin circular cover glass (11 mm in diameter) with one drop of saline was placed on top (Detmar et al., 1998; Milstone et al., 1998).

Dorsal Skin Chamber/Tumor Preparation

Dorsal skin chambers were implanted in mice using a procedure described elsewhere (Leunig et al., 1992). A small piece (1 mm diameter) of MCaIV (a murine mammary adenocarcinoma) or HCaI (a murine hepatocellular carcinoma) tumor tissue was implanted at the center of the dorsal chamber. Observations were made 1, 2, and 3 weeks after tumor implantation. The animals were positioned in a polycarbonate tube (inner diameter, 25 mm), and the chamber was fixed on the microscope stage.

Intravital Microscopy

The wound or the tumor was observed under an intravital fluorescence microscope (Axioplan, Zeiss, Oberkochen, Germany) (Fukumura et al., 1997). A fluorescence filter set for fluoroscein (Omega Optical, Brattleboro, VT) was used for GFP fluorescence images. The transilluminated image and the fluorescence image were either visualized by an intensified charge-coupled device (CCD) video camera (C2400–88, Hamamatsu Photonics K. K., Hamamatsu, Japan) and digitized using an image processing system (Global Image, Data Translation, Inc., Marlboro, MA) or photographed using Kodak 400 ASA film. Confocal images were acquired with an intravital fluorescence microscope (BH-2, Olympus America Inc., Melville, NY) equipped with a confocal laser scanning system (MRC-600; Bio-Rad Laboratories, Richmond, CA).

GFP Half-Life

The U87 glioblastoma and LS174T colon carcinoma cell lines were transfected with an expression construct bearing an engineeered GFP coding sequence under the control of a tetracycline-responsive promoter in a plasmid that also constitutively expresses the tetR-VP16 chimeric transcriptional activator. Clones showing low background and good induction were selected, and 5×10^4 cells grown in the absence of tetracycline (induced condition) were introduced into each well of a 6-well plate (35 mm diameter). Cells were propagated in the presence of tetracycline, 0.5 μg/ml, with the medium changed daily. For analysis the cells were lysed and the lysate subjected to spectrofluorimetry.

Preparation and Analysis of Mouse Embryo Fibroblasts

Embryos were harvested at day 18 postconception. Individual embryos were minced and incubated in complete medium. Embryo samples were retained for blot analysis for the presence or absence of the transgene, which was concordant with GFP expression. Primary fibroblasts were prepared for cytometry by trypsinization, washing in PBS, and fixation with 2% formaldehyde.

Histology and Immunohistochemistry

Tissue from the wound and tumor with adjacent tissue were surgically removed and embedded in OCT, snap frozen in liquid nitrogen (LN_2), and stored at −70°C. For immunohistology, rapid freezing using isopentane precooled in LN_2 of tissue embedded in gum tragacanth was also used. For conventional histology, tissue samples were fixed in 10% buffered formalin and embedded in paraffin. Sections were stained by avidin biotin complex methods as described previously (Cerf-Bensussan et al., 1983; Hollander et al., 1995). Tissue sections (4 μm) were air-dried for 10 min, fixed in acetone, and air-dried again for 10 min. Sections were then incubated in primary rabbit polyclonal antibodies to GFP (Clontech 1:100) for 1 hr. Secondary antibodies that were biotin- and cy3/5-labeled were used to detect primary antibody staining for immunohistochemistry and confocal microscopy, respectively. Each step was followed by three washes in phosphate-buffered saline. The sections were then incubated with ABC reagent, followed by postfixation in 2% paraformaldehyde, and counter stained with hematoxylin.

Electron Microscopy

Tissues from four mice were processed for electron microscopy. They were fixed in Karnovsky II solution and stored in sodium cacodylate buffer. They were then postfixed in osmium tetroxide, stained en bloc with uranyl acetate, dehydrated in graded ethanol solutions, infiltrated with propylene oxide/epoxy resin, and embedded in epoxy resin. One micrometer sections were cut, stained with toluidine blue, and examined by light microscopy. Representative sections were chosen for thin sectioning. Thin sections were cut, stained with lead citrate, and examined in a Philips 301 electron microscope.

Acknowledgments

We thank Michael Irizary, Andrew Rosenberg, Atul Bhan, and G. Richard Dickersin for suggestions and review of pathology; Dennis Brown for help with intravital confocal microscopy; Ben Leader for contributions to vector development; Bob Melder for assistance with flow cytometry; and Brian Stoll for analysis of GFP decay kinetics. This work was supported by NIH grants R35-CA-56591 to R. K. J. and DK43031 and AI27849 to B. S. Additional funds were provided by a grant to the Massachusetts General Hospital from Hoechst AG. D. F. is a Whitaker Fellow, and R. X. is supported by AI01472 and the Center for Inflammatory Bowel Disease.

Received May 12, 1998; revised August 7, 1998.

References

Berse, B., Brown, L.F., Van de Water, L., Dvorak, H.F., and Senger, D.R. (1992). Vascular permeability factor (vascular endothelial growth factor) gene is expressed differentially in normal tissues, macrophages, and tumors. Mol. Biol. Cell *3*, 211–220.

Boehm, T., Folkman, J., Browder, T., and O'Reilly, M.S. (1997). Antiangiogenic therapy of experimental cancer does not induce acquired drug resistance. Nature *390*, 404–407.

Bondár, I., Uhl, E., Barker, J.H., Galla, T.J., Hammersen, F., and Messmer, K. (1991). A new model for studying microcirculatory changes during dermal wound healing. Res. Exp. Med. *191*, 379–388.

Brown, L.F., Yeo, K.T., Berse, B., Yeo, T.K., Senger, D.R., Dvorak, H.F., and van de Water, L. (1992). Expression of vascular permeability factor (vascular endothelial growth factor) by epidermal keratinocytes during wound healing. J. Exp. Med. *176*, 1375–1379.

Cerf-Bensussan, N., Schneeberger, E.E., and Bhan, A.K. (1983). Immunohistologic and immunoelectron microscopic characterization of the mucosal lymphocytes of human small intestine by the use of monoclonal antibodies. J. Immunol. *130*, 2615–2622.

Cormack, B.P., Valdivia, R.H., and Falkow, S. (1996). FACS-optimized mutants of the green fluorescent protein (GFP). Gene *173*, 33–38.

Damert, A., Machein, M., Breier, G., Fujita, M.Q., Hanahan, D., Risau, W., and Plate, K.H. (1997). Up-regulation of vascular endothelial growth factor expression in a rat glioma is conferred by two distinct hypoxia-driven mechanisms. Cancer Res. *57*, 3860–3864.

Detmar, M., Brown, L.F., Schön, M.P., Elicker, B.M., Richard, L., Velasco, P., Fukumura, D., Monsky, W., Claffey, K.P., and Jain, R.K. (1998). Tortuous blood vessels and enhanced leukocyte-adhesion in VEGF transgenic mice. Invest. Dermatol. in press.

Dvorak, H.F. (1986). Tumors: wounds that do not heal. Similarities

between tumor stroma generation and wound healing. N. Engl. J. Med. *315*, 1650–1659.

Dvorak, H.F., Brown, L.F., Detmar, M., and Dvorak, A.M. (1995). Vascular permeability factor/vascular endothelial growth factor, microvascular hyperpermeability, and angiogenesis. Am. J. Pathol. *146*, 1029–1039.

Ferrara, N., and Davis-Smyth, T. (1997). The biology of vascular endothelial growth factor. Endocr. Rev. *18*, 4–25.

Fidler, I.J. (1995). Modulation of the organ microenvironment for treatment of cancer metastasis. J. Natl. Cancer Inst. *87*, 1588–1592.

Fleenor, D.E., and Kaufman, R.E. (1993). Characterization of the DNase I hypersensitive site 3′ of the human beta globin gene domain. Blood *81*, 2781–2790.

Frank, S., Hubner, G., Breier, G., Longaker, M.T., Greenhalgh, D.G., and Werner, S. (1995). Regulation of vascular endothelial growth factor expression in cultured keratinocytes. Implications for normal and impaired wound healing. J. Biol. Chem. *270*, 12607–12613.

Friesel, R.E., and Maciag, T. (1995). Molecular mechanisms of angiogenesis: fibroblast growth factor signal transduction. FASEB J. *9*, 919–925.

Fukumura, D., Yuan, F., Endo, M., and Jain, R.K. (1997). Role of nitric oxide in tumor microcirculation: blood flow, vascular permeability, and leukocyte-endothelial interactions. Am. J. Pathol. *150*, 713–725.

Gossen, M., and Bujard, H. (1992). Tight control of gene expression in mammalian cells by tetracycline-responsive promoters. Proc. Natl. Acad. Sci. USA *89*, 5547–5551.

Graeber, T.G., Peterson, J.F., Tsai, M., Monica, K., Fornace, A.J., Jr., and Giaccia, A.J. (1994). Hypoxia induces accumulation of p53 protein, but activation of a G1-phase checkpoint by low-oxygen conditions is independent of p53 status. Mol. Cell. Biol. *14*, 6264–6277.

Guy, C.T., Muthuswamy, S.K., Cardiff, R.D., Soriano, P., and Muller, W.J. (1994). Activation of the c-Src tyrosine kinase is required for the induction of mammary tumors in transgenic mice. Genes Dev. *8*, 23–32.

Haas, J., Park, E.C., and Seed, B. (1996). Codon usage limitation in the expression of HIV-1 envelope glycoprotein. Curr. Biol. *6*, 315–324.

Hanahan, D. (1997). Signaling vascular morphogenesis and maintenance. Science *277*, 48–50.

Hanahan, D., and Folkman, J. (1996). Patterns and emerging mechanisms of the angiogenic switch during tumorigenesis. Cell *86*, 353–364.

Heim, R., and Tsien, R.Y. (1996). Engineering green fluorescent protein for improved brightness, longer wavelengths and fluorescence resonance energy transfer. Curr. Biol. *6*, 178–182.

Helmlinger, G., Yuan, F., Dellian, M., and Jain, R.K. (1997). Interstitial pH and pO2 gradients in solid tumors in vivo: high-resolution measurements reveal a lack of correlation. Nat. Med. *3*, 177–182.

Hlatky, L., Tsionou, C., Hahnfeldt, P., and Coleman, C.N. (1994). Mammary fibroblasts may influence breast tumor angiogenesis via hypoxia-induced vascular endothelial growth factor up-regulation and protein expression. Cancer Res. *54*, 6083–6086.

Hollander, G.A., Simpson, S.J., Mizoguchi, E., Nichogiannopoulou, A., She, J., Gutierrez-Ramos, J.C., Bhan, A.K., Burakoff, S.J., Wang, B., and Terhorst, C. (1995). Severe colitis in mice with aberrant thymic selection. Immunity *3*, 27–38.

Jain, R.K. (1997). The Eugene M. Landis Award Lecture. Delivery of molecular and cellular medicine to solid tumors. Microcirculation *4*, 1–23.

Kerbel, R.S. (1991). Inhibition of tumor angiogenesis as a strategy to circumvent acquired resistance to anti-cancer therapeutic agents. Bioessays *13*, 31–36.

Kim, K.J., Li, B., Winer, J., Armanini, M., Gillett, N., Phillips, H.S., and Ferrara, N. (1993). Inhibition of vascular endothelial growth factor-induced angiogenesis suppresses tumour growth in vivo. Nature *362*, 841–844.

Leunig, M., Yuan, F., Menger, M.D., Boucher, Y., Goetz, A.E., Messmer, K., and Jain, R.K. (1992). Angiogenesis, microvascular architecture, microhemodynamics, and interstitial fluid pressure during early growth of human adenocarcinoma LS174T in SCID mice. Cancer Res. *52*, 6553–6560.

Levy, A.P., Levy, N.S., and Goldberg, M.A. (1996). Post-transcriptional regulation of vascular endothelial growth factor by hypoxia. J. Biol. Chem. *271*, 2746–2753.

Milstone, D.S., Fukumura, D., Padgen, R.C., O'Donnell, P.E., Davis, V.M., Benavidez, O.J., Monsky, W.L., Melder, R.J., Jain, R.K., and Gimbrone, J.M.A. (1998). Mice lacking E-selectin show normal numbers of rolling leukocytes but reduced leukocyte stable arrest on cytokine-activated microvascular endothelium. Microcirculation in press.

Parangi, S., O'Reilly, M., Christofori, G., Holmgren, L., Grosfeld, J., Folkman, J., and Hanahan, D. (1996). Antiangiogenic therapy of transgenic mice impairs de novo tumor growth. Proc. Natl. Acad. Sci. USA *93*, 2002–2007.

Risau, W. (1997). Mechanisms of angiogenesis. Nature *386*, 671–674.

Schmaltz, C., Hardenburgh, P.H., Wells, A., and Fisher, D.E. (1998). Regulation of proliferation-survival decisions during tumor cell hypoxia. Mol. Cell. Biol. *18*, 2845–2854.

Shima, D.T., Deutsch, U., and D'Amore, P.A. (1995). Hypoxic induction of vascular endothelial growth factor (VEGF) in human epithelial cells is mediated by increases in mRNA stability. FEBS Lett. *370*, 203–208.

Shweiki, D., Itin, A., Soffer, D., and Keshet, E. (1992). Vascular endothelial growth factor induced by hypoxia may mediate hypoxia-initiated angiogenesis. Nature *359*, 843–845.

Stein, I., Neeman, M., Shweiki, D., Itin, A., and Keshet, E. (1995). Stabilization of vascular endothelial growth factor mRNA by hypoxia and hypoglycemia and coregulation with other ischemia-induced genes. Mol. Cell. Biol. *15*, 5363–5368.

Tischer, E., Mitchell, R., Hartman, T., Silva, M., Gospodarowicz, D., Fiddes, J.C., and Abraham, J.A. (1991). The human gene for vascular endothelial growth factor. Multiple protein forms are encoded through alternative exon splicing. J. Biol. Chem. *266*, 11947–11954.